Detection of low-concentration superparamagnetic nanoparticles using an integrated radio frequency magnetic biosensor

J. Devkota, C. Wang, A. Ruiz, S. Mohapatra, P. Mukherjee et al.

Related Articles

Piezoelectric resonators based on self-assembled diphenylalanine microtubes
Appl. Phys. Lett. 102, 073504 (2013)

Slow light enhanced sensitivity of resonance modes in photonic crystal biosensors
Appl. Phys. Lett. 102, 041111 (2013)

A pillar-based microfilter for isolation of white blood cells on elastomeric substrate
Biomicrofluidics 7, 014102 (2013)

The effects of diffusion on an exonuclease/nanopore-based DNA sequencing engine
J. Chem. Phys. 137, 214903 (2012)

Nanogap-based dielectric-specific colocalization for highly sensitive surface plasmon resonance detection of biotin-streptavidin interactions
Appl. Phys. Lett. 101, 233701 (2012)

Additional information on J. Appl. Phys.

Detection of low-concentration superparamagnetic nanoparticles using an integrated radio frequency magnetic biosensor

J. Devkota,[1] C. Wang,[2] A. Ruiz,[1] S. Mohapatra,[2] P. Mukherjee,[1] H. Srikanth,[1] and M. H. Phan[1,a)]

[1]Department of Physics, University of South Florida, Tampa, Florida 33620, USA
[2]Department of Molecular Medicine, University of South Florida, Tampa, Florida 33612, USA

Improving the sensitivity of existing biosensors for highly sensitive detection of magnetic nanoparticles as biomarkers in biological systems is an important and challenging task. Here, we propose a method of combining the magneto-resistance (MR), magneto-reactance (MX), and magneto-impedance (MI) effects to develop an integrated magnetic biosensor with tunable and enhanced sensitivity. A systematic study of the 7 nm Fe_3O_4 nanoparticle concentration dependence of MR, MX, and MI ratios of a soft ferromagnetic amorphous ribbon shows that these ratios first increase sharply with increase in particle concentration (0–124 nM) and then remain almost unchanged for higher concentrations (124 nM–1240 nM). The MX-based biosensor shows the highest sensitivity. With this biosensor, $\sim 2.1 \times 10^{11}$ 7 nm Fe_3O_4 nanoparticles can be detected over a detection area of $2.0 \times 10^5 \, \mu m^2$, which is comparable to a superconducting quantum interference device biosensor that detects the presence of $\sim 1 \times 10^8$ 11 nm Fe_3O_4 nanoparticles over a detection area of $6.8 \times 10^4 \, \mu m^2$. The proposed biosensor can detect low and various concentrations of superparamagnetic nanoparticles (below 10 nm in size), which is of practical importance in biosensing applications. © 2013 American Institute of Physics. [http://dx.doi.org/10.1063/1.4795134]

I. INTRODUCTION

Recent attention has been drawn to a new class of highly sensitive magnetic sensor based on the giant magneto-impedance (GMI) effect.[1–3] GMI refers to a large change in the ac impedance ($Z = R + jX$, where R and X are the ac resistance and reactance, respectively) of a magnetic conductor subject to a dc magnetic field, and it has been observed in a number of soft ferromagnetic materials, including magnetic wires,[4] ribbons,[5] and thin films.[6] Importantly, magnetic sensors based on GMI technology operate at room temperature, with ultrahigh sensitivity (detectable fields, ~ 100 pT), high thermal stability, high spatial resolution, small size, light weight, and low power consumption.[2,3,7] These sensors are used in today's mobile phones and electronic devices.[1,7] The ultrahigh sensitivity of the GMI sensors also makes them very promising for biosensing purposes.[2,3,8,9]

The incorporation of GMI technology with magnetic nanoparticles provides a promising approach for detection of cancer cells and biomolecules.[10–18] This method relies on the magnetic fringe fields associated with magnetic nanoparticles embedded inside the cells to give a change in magneto-impedance from the normal response exhibited by the magnetic sensing element. A GMI biosensor prototype using a soft ferromagnetic amorphous ribbon was designed for detection of magnetic Dynabeads.[13] This type of sensor was then advanced for detecting Au-coated Fe_3O_4 nanoparticles embedded inside human embryonic kidney (HEK 293) cells.[15] Recently, a GMI-based microchannel system has been successfully developed for quick and parallel genotyping of

human papilloma virus type 16/18 and for targeted detection of gastric cancer cells.[16,17] Despite these studies, research in this field is still in its infancy, and there is an increasing need for improving the field sensitivity of existing GMI biosensors.[18] In particular, two very important questions emerge and need to be addressed: (i) Can a GMI biosensor detect superparamagnetic nanoparticles at different concentrations? (ii) Can GMI-based techniques achieve sensitivity levels comparable to those of existing biosensors?

To address these important issues, we have performed a systematic study of the influence of magnetic particle (Fe_3O_4, mean size ~ 7 nm) concentration on the ac magneto-resistance (MR), magneto-reactance (MX), and magneto-impedance (MI) effects of an amorphous METGLAS® 2714A ribbon. While previous efforts have been focused mainly on developing a biosensor based on the MI effect which has limited sensitivity,[10–18] we show that by exploiting the MR and MX effects it is possible to improve the sensitivity of the biosensor by up to 50% and 100%, respectively. The MX-based approach shows the most sensitive detection of superparamagnetic nanoparticles at low concentrations, demonstrating a sensitivity level comparable to that of a superconducting quantum interference device (SQUID)-based biosensor. Unlike a SQUID, however, the proposed MX technique is cryogen-free and operates at room temperature, providing a promising avenue to the development of low-cost highly sensitive biosensors.

II. EXPERIMENT

Superparamagnetic iron oxide (SPIO) nanoparticles were prepared by a chemical method, and have been reported to have great potential for drug delivery, magnetic resonance

---

a)Author to whom correspondence should be addressed. Electronic mail: phanm@usf.edu.

imaging (MRI), and other biomedical applications.[19] The water soluble SPIO nanoparticles were prepared by adding SPIO nanoparticles hexane dispersion (40 mg in 0.2 ml) to a tetramethylammonium 11-aminoundecanoate suspension in dichloromethane (40 mg in 2 ml). The mixture was shaken for overnight and the precipitate was separated using a magnet and washed with dichloromethane. The resulting SPIO NPs were dispersed in deionized water. The composition of the material was confirmed to be Fe_3O_4 with an average size of 7 nm by X-ray diffraction (XRD) and transmission electron microscopy (TEM). The inset of Fig. 1 shows a typical TEM image confirming the monodisperse nature of the as-synthesized nanoparticles. The magnetic properties of the nanoparticles were measured using a SQUID. The room temperature superparamagnetic nature of the SPIO particles is evident as a magnetic hysteresis (M-H) loop taken at 300 K (Fig. 1) shows the absence of remanent magnetization and zero coercivity. The SPIO nanoparticles suspended in water were drop-casted onto the surface of the sensing element of a biosensor prototype before conducting each magneto-impedance measurement. A biosensor prototype was designed by using an amorphous METGLAS® 2714A ribbon of dimension 16 mm × 2 mm × 0.015 mm and composition $Co_{65}Fe_4Ni_2Si_{15}B_{14}$ as a magnetic sensing element. The ribbons were produced by a melt-spinning technique and provided by Metglas/Hitachi Metals America. The ribbon piece was fixed on a non-magnetic glass support and placed at the center of a Helmholtz coil that provided a dc magnetic field ranging up to ±120 Oe and parallel to its length. A driving current of magnitude 5 mA over the frequency range of 0.1–13 MHz was supplied along the ribbon axis, and the dc magnetic field-induced MI, MR, and MX changes were measured by a four-probe technique on a HP4192A impedance analyzer over a 1 mm segment of ribbon at room temperature. These measurements were performed after drop-casting 20 μl of various concentrations (0, 0.124 nM, 1.24 nM, 12.4 nM, 62 nM, 124 nM, 360 nM, 620 nM, 940 nM, and 1240 nM) of SPIO nanoparticles in water and compared to the measurement for a blank prototype. A thin parafilm paper was used to avoid a direct contact between the SPIO nanoparticles and the ribbon surface. The change in MR, MX, and MI with the applied field at a given frequency of the driving current (defined as the MR, MX, and MI ratios) was calculated by using the following respective equations:
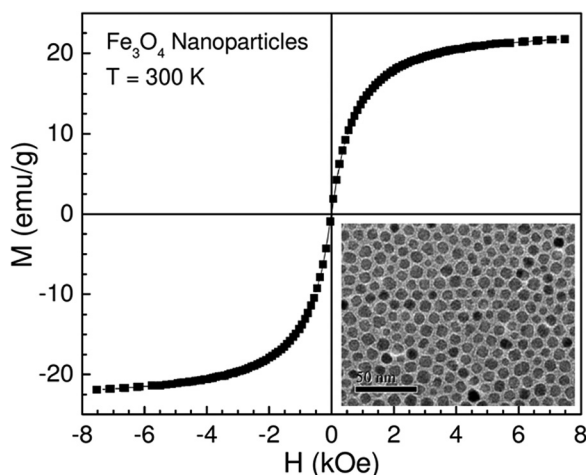
$$\frac{\Delta R}{R} = \frac{R(H) - R(H_{max})}{R(H_{max})} \times 100\%, \tag{1}$$

$$\frac{\Delta X}{X} = \frac{X(H) - X(H_{max})}{X(H_{max})} \times 100\%, \tag{2}$$

$$\frac{\Delta Z}{Z} = \frac{Z(H) - Z(H_{max})}{Z(H_{max})} \times 100\%. \tag{3}$$

The changes in the MR, MX, and MI ratios due to the presence of SPIO nanoparticles at different concentrations were obtained by subtracting the corresponding responses observed for the blank prototype as

$$\Delta\eta_\xi = [\xi]_{max,\,SPIO} - [\xi]_{max,\,Blank}, \tag{4}$$

where $[\xi]_{max}$ with $\xi = \frac{\Delta R}{R}$, $\frac{\Delta X}{X}$, and $\frac{\Delta Z}{Z}$ are the maximum values of the MR, MX, and MI ratios in Eqs. (1)–(3), respectively. This parameter is considered an important figure-of-merit for assessing the sensitivity of the biosensor.

III. RESULTS AND DISCUSSION

To assess the full potential of the sensor detection, we first investigated the magnetic field and frequency dependences of MR, MX, and MI ratios of the plain ribbon and used this prototype as a background in order to determine the effects of the fringe fields introduced by the SPIO suspensions. Figures 2(a)–2(c) show these dependences for the blank ribbon prototype, covered with a parafilm paper. It is observed that with increasing frequency the MR and MI ratios first increased, reached their maximum values at ~6 MHz and ~1.5 MHz, respectively, and finally decreased for higher frequencies. This can be associated with the relative contributions to the permeability and hence magneto-impedance from the domain wall motion at low frequency range and the spin rotation at high frequency range.[1] The MR and MI curves showed a single peak at zero field with a height that decreased with increasing dc field at low frequencies ($f < 1$ MHz); however, a double-peak feature with a clear dip at zero field was observed at higher frequencies ($f \geq 1$ MHz). The variation from the single-peak to double-peak structure in MR and MI curves around 1 MHz can also be attributed to the two magnetization processes that take place in the sample; domain wall motion dominates at low frequency ($f < 1$ MHz) while spin rotation is responsible for at high frequency ($f \geq 1$ MHz). The MX profiles showed a different behavior; the MX ratio decreased with increasing frequency and the MX curves showed a double-peak structure over the entire frequency range of 0.1–13 MHz, implying the dominance of a transverse magnetic anisotropy in the Co-based ribbon.[1] A similar trend was observed for the case of the ribbon with SPIO nanoparticles, the origin of which has been well documented in our previous study.[20] Note that the MX ratio is largest at low frequency range, while the

FIG. 1. Magnetic hysteresis loop of 7 nm Fe_3O_4 nanoparticles taken at 300 K; Inset shows a typical TEM image of the nanoparticles.

(a)

(b)

(c)
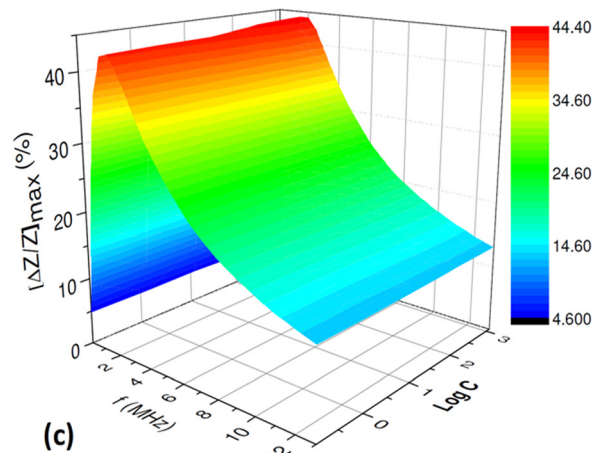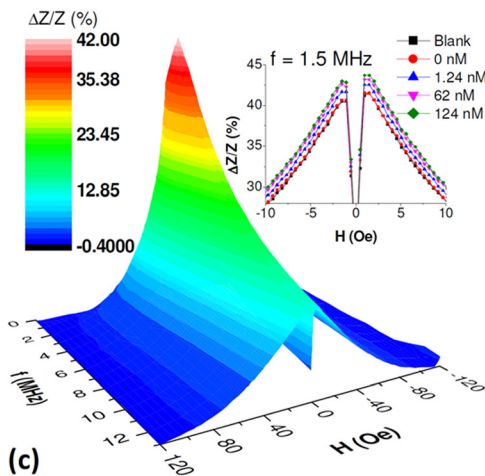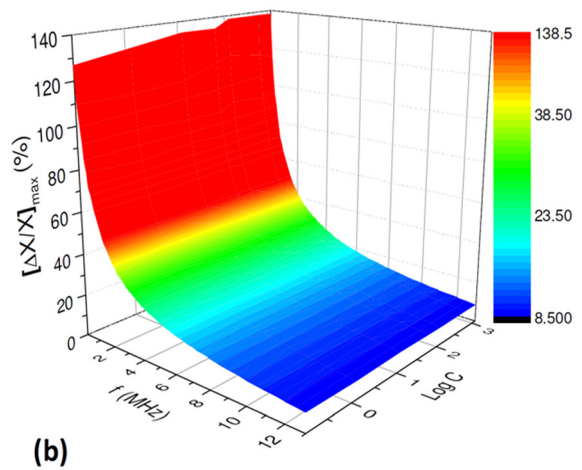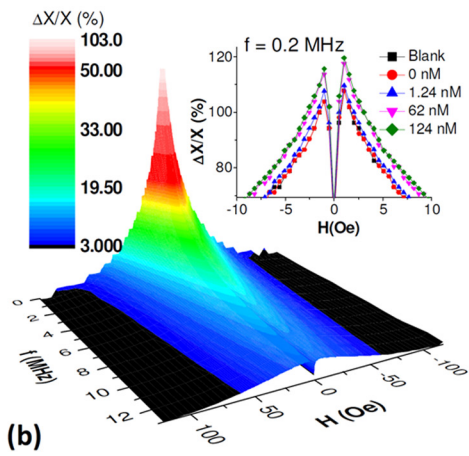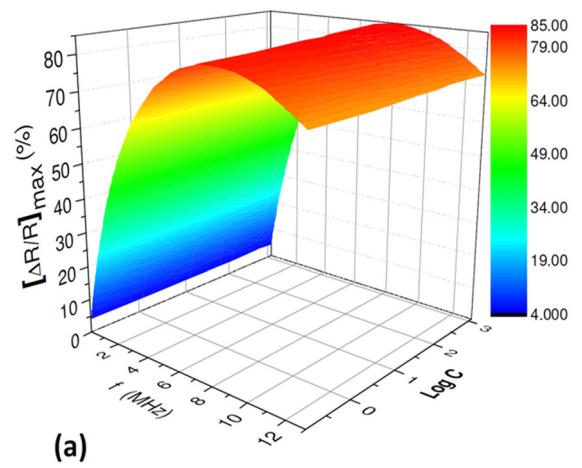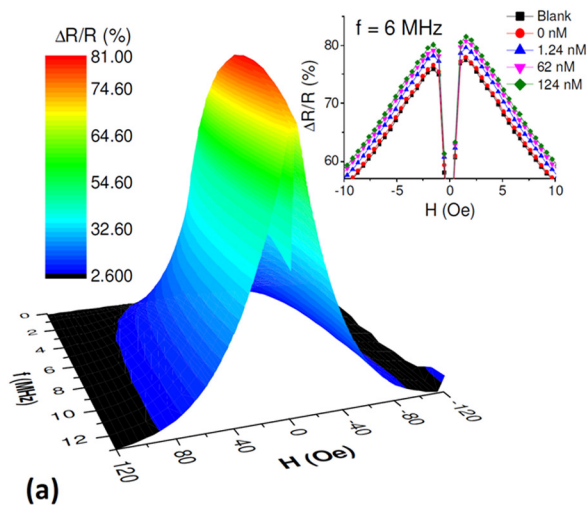
FIG. 2. 3D plots of the magnetic field and frequency dependences of MR (a), MX (b), and MI (c) ratios for the blank ribbon covered by a parafilm paper. Insets of (a)–(c) show the MR, MX, and MI profiles for the blank prototype and different concentrations of SPIO nanoparticles.

(a)

(b)

(c)

FIG. 3. 3D plots of the particle concentration and frequency dependences of MR, MX, and MI ratios.

largest MR ratio is obtained at high frequency range. This can be understood by considering the corresponding contributions to the impedance from the reactance at low frequency range and the resistance at high frequency range.[20] As compared to the MI ratio, the larger values of the MR and MX ratios are expected to make them more sensitive in detecting the fringe magnetic fields of SPIO nanoparticles located on the surface of the ribbon.

Insets of Figs. 2(a)–2(c) present the magnetic field dependence of MR, MX, and MI ratios at selected frequencies for the blank prototype and different concentrations of SPIO nanoparticles in water. There was no significant change in

the MR, MX, and MI ratios of the ribbon when 20 μl of water was drop-casted on its surface. However, the presence of the SPIO nanoparticles resulted in clear increases in the MR, MX, and MI ratios. Such increases are due to the disturbances on the applied dc longitudinal and ac transverse magnetic fields by the fringe magnetic fields of the magnetic particles.[11]

Figure 3 shows the dependence of the MR, MX, and MI ratios on SPIO nanoparticle concentration in the frequency range 0.1–13 MHz. It is observed that the frequency dependences of the MR, MX, and MI ratios for all tested concentrations of the SPIO particles follow a similar trend to the blank sample. At a given frequency, there were clear increases in the MR, MX, and MI ratios with the concentration of the SPIO particles in the range 0–124 nM. To best probe such changes, we have performed a quantitative analysis of modification on the MR, MX, and MI responses due to the presence of the SPIO nanoparticles at selected frequencies of 6 MHz, 0.1 MHz, and 1.5 MHz, where their corresponding largest ratios were achieved. We have evaluated the difference in maximum of the MR, MX, and MI ratios by subtracting their values for the blank ribbon covered by the parafilm paper from the corresponding values for a SPIO sample of particular concentration as given in Eq. (4). As expected, for the ribbon with only water no change in the MR, MX, and MI ratios was observed ($\Delta \eta \approx 0$). However, these ratios first increased sharply with increase in particle concentration from 0 to 124 nM and then remained almost unchanged for higher particle concentrations (≥ 124 nM). The change in MI [$\Delta \eta_{(\Delta Z/Z)}$] was the smallest, whereas the largest change in MX [$\Delta \eta_{(\Delta X/X)}$] was achieved. The maximum changes in the MI, MR, and MX ratios are determined to be about 2.65%, 4.51%, and 11.54%, respectively. This value of $\Delta \eta_{(\Delta X/X)}$ is about 2.5 and 5 times (50% and 100%, correspondingly) greater than those of $\Delta \eta_{(\Delta R/R)}$ and $\Delta \eta_{(\Delta Z/Z)}$, respectively. This important finding indicates that the changes in the components of the MI (magneto-resistance and magneto-reactance) are more promising for detection of low-concentration superparamagnetic nanoparticles in a biological system than the change in magneto-impedance itself.

The above results can be interpreted by considering the disturbance of the applied dc longitudinal and ac transverse
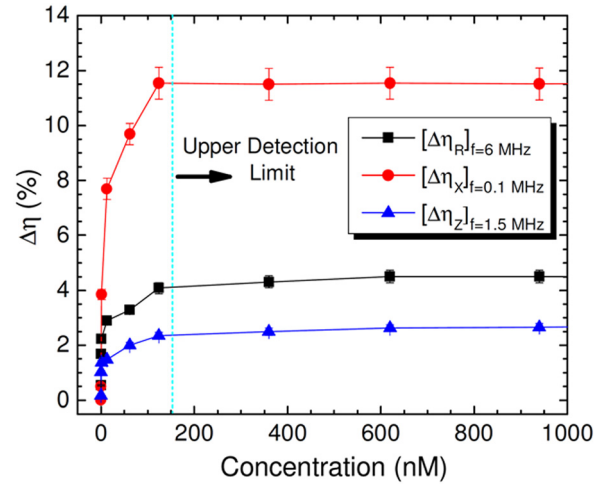
FIG. 4. Relative SPIO particle concentration dependence of MR, MX, and MI showing the sensitivity and upper limit of the detection of the biosensor.

fields due to the presence of the fringe magnetic fields of the SPIO nanoparticles on the ribbon surface. As the concentration of SPIO nanoparticles is increased, the strength of fringe fields also increases, thus disturbing the dc and ac magnetic fields on the ribbon to a greater degree and consequently altering the MR, MX, and MI. In the present case, the increases of $\Delta \eta_{(\Delta R/R)}$, $\Delta \eta_{(\Delta X/X)}$, and $\Delta \eta_{(\Delta Z/Z)}$ with increasing concentration of SPIO nanoparticles (Fig. 4) can be attributed to the increase of transverse permeability due to the coupling of the magnetic fringe fields of the nanoparticles with the ac transverse magnetic field. This coupling becomes independent of SPIO nanoparticles as the concentration of nanoparticles exceeds a critical concentration (which is ~124 nM in the present case). As a result, no further increase in the $\Delta \eta$ is obtained. Clearly, the concentration of ~124 nM sets an upper limit of the sensor detection of 7 nm Fe_3O_4 nanoparticles (Fig. 4).

Finally, to compare the sensitivity of the proposed biosensor with those of existing biosensors, we summarize in Table I the important parameters of various magnetic biosensors. From a biosensor perspective, we recall the importance of distinguishing the density of labels within a detection area from the number of labels, since the smaller the detection

TABLE I. Detection of magnetic particles using different biosensors.

Detector type	Detection area (μm^2)[b]	Particle	Particle diameter (μm)	Sensitivity (particles)	Area per detectable particle (μm^2)	Reference
GMI	2.0×10^5	Magnetite	7[a,c]	2.1×10^{11}	2.0×10^{-6}	Present
SQUID	6.8×10^4	Magnetite	11[a]	1×10^8	6.8×10^{-4}	22
Microcantilever	2×10^4	NdFeBLa	2	1	2.0×10^4	23
BARC III	3.1×10^4	Ni_3Fe_{70}	3.3	1	3.1×10^4	21
Resonant coil	2.5×10^7	Dynal M-280	2.8	1×10^5	2.5×10^2	24
Spin valve	12	Micromer®-M	2	1	12	25
AMR ring	8	$Ni_{30}Fe_{70}$	4.3	1	8	26
Hall sensor	5.8	Dynal M-280	2.8	1	5.8	27

[a]Measured in nanometer.
[b]Surface area of the sensor used to capture the magnetic particles and detect them.
[c]Not coated with polymer.

area, the less sensitive the biochemical assay.[21] Therefore, the sensitivity figure-of-merit is the sensing area required per detectable magnetic particle. As one can see clearly in Table I for the detection limit of nanoscale particles, the present biosensor can detect approximately 2.1×10^{11} 7 nm Fe_3O_4 nanoparticles over a detection area of $2.0 \times 10^5 \ \mu m^2$, which is comparable to a SQUID-based biosensor[22] that detects the presence of $\sim 1 \times 10^8$ 11 nm Fe_3O_4 nanoparticles over a detection area of $6.8 \times 10^4 \ \mu m^2$. As compared to the SQUID biosensor, the present biosensor has advantages of room-temperature operation, less complex instruments, and hence more portable and flexible implementation. Therefore, the proposed biosensor is very promising for highly sensitive detection of superparamagnetic nanoparticles as magnetic markers in biological systems. We are now in process of exploiting this biosensor for detection and identification of different types of cancer cells that have taken up surface-functionalized SPIO nanoparticles.

IV. CONCLUSIONS

We have demonstrated the possibility of combining the ac magneto-resistance, magneto-reactance, and magneto-impedance effects to develop an integrated magnetic biosensor with tunable and enhanced sensitivity. The magneto-reactance based biosensor shows the highest sensitivity, which is comparable to that of a SQUID-based biosensor. The proposed biosensor can detect superparamagnetic nanoparticles (less than 10 nm in size) at various and low particle concentrations, which is of practical importance in biosensing applications.

[1]M. H. Phan and H. X. Peng, Prog. Mater. Sci. **53**, 323 (2008).

[2]T. Uchiyama, S. Nakayama, K. Mohri, and K. Bushida, Phys. Status Solidi A **206**, 639 (2009).

[3]S. Nakayama, S. Atsuta, T. Shinmi, and T. Uchiyama, Biosens. Bioelectron. **27**, 34 (2011).

[4]V. Zhukova, M. Ipatov, and A. Zhukov, Sensors **9**, 9216 (2009).

[5]M. H. Phan, H. X. Peng, M. R. Wisnom, and S. C. Yu, J. Appl. Phys. **98**, 014316 (2005)

[6]T. Morikawa, Y. Nishibe, and H. Yamadera, IEEE Trans. Magn. **33**, 4367 (1997).

[7]K. Mohri and Y. Honkura, Sens. Lett. **5**, 267 (2007).

[8]H. Chiriac, D. D. Herera, and S. Corodeanu, J. Magn. Magn. Mater. **311**, 425 (2007).

[9]S. Nakayama, K. Sawamura, K. Mohri, and T. Uchiyama, PLoS ONE **6**, e25834 (2011).

[10]T. Kanno, K. Mohri, T. Yagi, T. Uchiyama, and L. P. Shen, IEEE Trans. Magn. **33**, 3358 (1997)

[11]G. V. Kurlyandskaya, M. L. Sanchez, B. Hernando, V. M. Prida, P. Gorria, and M. Tejedor, Appl. Phys. Lett. **82**, 3053 (2003).

[12]H. Chiriac, M. Tibu, A. E. Moga, and D. D. Herea, J. Magn. Magn. Mater. **293**, 671 (2005).

[13]G. Kurlyandaya and V. Levit, Biosens. Bioelectron. **20**, 1611 (2005).

[14]F. Blanc-Beguin, S. Nabily, J. Gieraltowski, A. Turzo, S. Querellou, and P. Y. Salaun, J. Magn. Magn. Mater. **321**, 192 (2009).

[15]A. Kumar, V. Fal-Miyar, J. A. Garcia, A. Cerdeira, S. Mohapatra, H. Srikanth, J. Gass, and G. V. Kurlyandskaya, Appl. Phys. Lett. **91**, 143902 (2007).

[16]H. Yang, L. Chen, C. Lei, J. Zhang, D. Li, Z. M. Zhou, C. C. Bao, H. Y. Hu, X. Chen, F. Cui, S. X. Zhang, Y. Zhou, and D. X. Cui, Appl. Phys. Lett. **97**, 043702 (2010).

[17]L. Chen, C. C. Bao, H. Yang, D. Li, C. Lei, T. Wang, H. Y. Hu, M. He, Y. Zhou, and D. X. Cui, Biosens. Bioelectron. **26**, 3246 (2011).

[18]G. Kurlyandaya, J. Magn. Magn. Mater. **321**, 659 (2009).

[19]C. Y. Wang, S. Ravi, G. V. Martinez, V. Chinnasamy, P. Raulji, M. Howell, Y. Davis, J. Mallela, M. S. Seehra, and S. Mohapatra, J. Controlled Release **163**, 82 (2012).

[20]J. Devkota, A. Ruiz, P. Mukherjee, H. Srikanth, M. H. Phan, A. Zhukov, and V. S. Larin, J. Alloys Compd. **549**, 295 (2013).

[21]J. C. Rife, M. M. Miller, P. E. Sheehan, C. R. Tamanaha, M. Tondra, and L. J. Whitman, Sens. Actuators A **107**, 209 (2003).

[22]S. Katsura, T. Yasuda, K. Hirano, A. Minzuno, and S. Tanaka, Supercond. Sci. Technol. **14**, 1131 (2001).

[23]D. R. Baselt, G. U. Lee, M. Natesan, S. W. Metzer, P. E. Sheehan, and R. Colton, Biosens. Bioelectron. **13**, 731 (1998).

[24]J. Richardson, A. Hill, R. Luxton, and P. Hawkins, Biosens. Bioelectron. **16**, 1127 (2001).

[25]D. L. Graham, H. Ferreira, J. Bernardo, P. P. Freitas, and J. M. S. Cabral, J. Appl. Phys. **91**, 7786 (2002).

[26]M. M. Miller, G. A. Prinz, S.-F. Cheng, and S. Bounnak, Appl. Phys. Lett. **81**, 2211 (2002).

[27]P.-A. Besse, G. Boero, M. Demierre, V. Pott, and R. Popovic, Appl. Phys. Lett. **80**, 4199 (2002).